β-Phase Stability of Two Biomedical β-Titanium Alloys During Severe Plastic Deformation

DOINA RADUCANU,[1] VASILE DANUT COJOCARU,[1]
ANNA NOCIVIN [ID],[2,3] ION CINCA,[1] NICOLAE SERBAN,[1]
and ELISABETA MIRELA COJOCARU[1]

1.—Faculty of Materials Science and Engineering, POLITEHNICA University of Bucharest, 313 Spl. Independentei, 060042 Bucharest, Romania. 2.—Faculty of Mechanical, Industrial and Maritime Engineering, Ovidius University of Constanta, 900527 Constanta, Romania. 3.—e-mail: anocivin@univ-ovidius.ro

The β-phase stability and deformation behavior patterns of two β-type titanium bioalloys, viz. Ti-Nb-Ta-Zr (TNTZ) type and Ti-Nb-Ta (TNT) type, processed by a series of intense plastic deformations have been investigated theoretically and experimentally. Firstly, theoretical analysis was carried out, including an estimation of possible deformation mechanisms based on the electronic parameters of the studied alloys identified with the aid of the Bo–Md diagram. Secondly, phase composition and structural parameters determined by x-ray diffraction (XRD) analysis revealed that the application of severe plastic deformation (SPD) induces grain refinement (in particular for one of the two alloys), accompanied by residual stress generation and some partial phase transformation. Scanning electron microscopy (SEM)/transmission electron microscopy (TEM) imaging and some measurements of the texture completed the deformation behavior analysis. TNT alloy, with higher β stability ($Mo_{eq} \sim 12.5$ wt.%), presented an almost unmodified β-grain dimension from 29.4 nm to 24.4 nm (and thus poor β-grain refinement), coupled with a very fine dispersion of nanometric (~ 8.4 nm) crystallites of orthorhombic α″-stress-induced martensite. TNTZ alloy, also with high β stability (Mo_{eq} 10.1 wt.%), showed accentuated β-grain refinement (from 27.8 nm to 9.9 nm), with a very small amount of orthorhombic α″-stress-induced martensite, but grain dimensions almost three times larger than that of the TNT alloy (~ 20.8 nm). The theoretical estimations concerning the possible deformation mechanisms are supported by the analysis of the experimental results.

INTRODUCTION

β-Type alloys are preferred biomaterials for permanent human bone implants due to their good mechanical and biochemical compatibility (high strength coupled with low elastic modulus), representing better alternatives to α- or α/β-type titanium alloys. Therefore, over the last decade, the development of β-titanium alloys with low elastic modulus comparable to that of human bone by using nontoxic alloying elements such as Nb, Ta, and Zr as β-stabilizers has become an interesting area of research in the bioimplant materials field.[1–7]

The mechanical biocompatibility of these alloys can be enhanced by solid-solution strengthening (by increasing the amount of solute alloying elements), precipitation of secondary phases, or grain refinement to nanoscale dimensions.[8,9] The efficiency of each of these methods depends on the requirements concerning the structural and mechanical properties of the alloy, which may vary as a function of the particular destination/location, dimensions, mechanical demands, and biochemical involvement of the implant. Generally, as a common denominator, high strength coupled with low elastic modulus and high biochemical compatibility with the human body are desirable; For example, low elastic modulus, more facile mechanical processing, and

enhanced biocompatibility can be obtained for a single β-phase structure, but with only moderate mechanical strength. However, to achieve this, good β-phase stability is required.[7–11]

If higher mechanical strength is desired, a structural state formed from a combination of two phases can be applied, viz. the β-phase with a certain amount of α'' martensitic phase induced by severe plastic deformation (SPD), which can be adjusted by selecting the degree of grain refinement.[10,11] It should be emphasized that this relies on achieving a small and controllable amount of secondary orthorhombic α'' martensitic phase, which has a lower Young's modulus in comparison with hexagonal α' martensite-or and ω-phase. Thus, for a low level of presence/precipitation of secondary phases, even if the elastic modulus increases slightly together with the mechanical strength, the overall mechanical biocompatibility is improved.[7–12] Therefore, the mechanical biocompatibility of β-phase Ti alloys can be increased under some special conditions by precipitation of the orthorhombic α'' martensitic phase,[13,14] depending on its dispersion, dimension, and quantity. Considering the combination of efficient grain refinement and stress-induced martensitic phase formation, this can be achieved by using various SPD procedures, including multipass rolling (MPR), accumulative roll bonding (ARB), equal-channel angular pressing (ECAP), and high-pressure torsion (HPT).[2–4] The mechanisms induced during SPD can generate dislocation slip, twinning, and formation of stress-induced martensite (SIM),[7] depending on the stability of the β-phase and the extent of deformation achieved.[1–4] By controlling the SPD procedure, the grain refinement of β-Ti alloys can lead to ultrafine (UFG) or even nanograin dimensions, which enhance the mechanical properties. However, during SPD, various other phases, such as α' or ω, may form in the β-matrix, having more or less beneficial influences. The formation of these phases depends on the stability of the β-phase.[8–17] Therefore, it is important to study the stability of the β-phase during SPD. To this end, two particular biomedical β-stabilized Ti alloys were studied in the work presented herein, viz. Ti-25Nb-25Ta (TNT) and Ti-29Nb-9Ta-10Zr (TNTZ) (wt.%).

Besides the addition of a large amount of alloying elements[8,9] to strengthen the β solid solution (48% alloying elements for the TNTZ alloy and 50% for the TNT alloy), these two alloys were also subjected to grain refinement and/or stress-induced phase transformations via SPD, as an additional method for mechanical biocompatibility enhancement. SPD can induce formation of a certain amount of α'' martensitic phase depending on the β-phase stability. The combination of β and α'' phases was evaluated for the two studied alloys: firstly theoretically, using the Bo–Md diagram first provided by Morinaga[15] and later extended by Abdel Hady et al.,[16] and then experimentally using XRD analysis and scanning electron microscopy (SEM)/transmission electron microscopy (TEM) imaging; the evolution of the structural parameters and phase stability during SPD was analyzed.

It should be underlined that the two studied alloys could clearly be considered separately due to their different chemical compositions and SPD methods applied. However, the two alloys are considered together herein for the following reasons: they are β-based titanium alloys (with a similar type of structure), both contain a high level of alloying elements ($\sim 50\%$) for strengthening the β solid solution, and both are processed by SPD with plastic strain above 2.0, ensuring that an SPD structural state is obtained in each case.

The aim of the theoretical analysis, depending on the nature of the electronic bonds,[15,16] is to reduce the effort usually associated with experimental alloy screening (melting, casting, homogenization, mechanical processing, and structural and mechanical characterization). Indeed, such theoretical predictions of the structure and mechanical behavior patterns can identify optimized routes for alloy design.

Regarding the experimental evaluation of the two studied alloys, the microstructural and textural investigation relied on XRD analysis, which provides sufficient data acquisition and processing, supplemented by relevant SEM/TEM imaging. This combination of experimental analysis coupled with theoretical estimations can provide a scientific contribution to establish, in the first instance, the conditions for β-phase stability during SPD.

EXPERIMENTAL PROCEDURES

Synthesis of Alloys

The nominal compositions of the two studied alloys (mass fraction) are as follows:

(a) Ti-29% Nb-9% Ta-10% Zr (wt.%) (48% of alloying elements)—TNTZ.
(b) Ti-25% Nb-25% Ta (wt.%) (50% of alloying elements)—TNT.

The alloys were prepared using a levitation induction melting furnace (FIVE CELES—MP25) with nominal power of 25 kW and melting capacity of 30 cm^3, under high vacuum of 10^{-4} mbar to 10^{-5} mbar as protective atmosphere. The alloy synthesis was conducted under high vacuum and intense agitation of the melted alloy. The ingots were remelted twice to achieve a high degree of chemical homogeneity.

Thermomechanical Processing (TMP) of the Two β-Ti Alloys

After synthesis, the two alloys were thermomechanically processed to obtain precursor samples before SPD by homogenization thermal treatment (at 950°C for 6 h with air cooling), cold rolling (20

passes with ε_{tot} = 60%), and thermal recrystallization treatment (at 850°C for 30 min with water cooling). The homogenization temperature should usually be as high as possible to ensure efficient diffusion. The temperatures for the thermal treatments were selected by considering the β-transus temperature of around 700°C[3,18–21] and the recrystallization parameters[22] for similar types of alloy. After the thermal treatments, the precursor samples were subjected to SPD.

For the TNTZ alloy, five distinct steps of MPR were applied: (1) two passes with ε_{tot} = 20%, (2) four passes with ε_{tot} = 40%, (3) six passes with ε_{tot} = 60%, (4) eight passes with ε_{tot} = 80%, and (5) ten passes with ε_{tot} = 90%.

For the TNT alloy, four distinct steps/cycles of ARB were applied. The roll bonding in each cycle consisted of rolling two stacked metal sheets with equal dimensions with a deformation degree of 50% at a rolling rate of 1.2 m min^{-1}, thereby obtaining one final sheet with the same thickness as the initial two. The billet roll stand was pretensioned for a negative skip (–0.2 mm). The dimensions of the precursor sample used to initiate the ARB cycles were 0.1 mm × 8 mm × 70 mm. The number of layers obtained in each ARB cycle was 2, 4, 8, and 16, respectively. As a common feature for both alloys, after SPD (MPR or ARB) processing, the final plastic strain exceeded 2.0, a value corresponding to the SPD structural state. All the samples had small dimensions to enable experiments on laboratory scale. Extrapolation of these preliminary results to larger samples is possible, by technologic transfer. All mechanical processing steps were performed using a Mario Di Maio LQR120AS laboratory mill.

Microstructural Analysis

A Metkon MICRACUT 200 type machine, with diamond cutting disks, was used for cutting. The specimens were then fixed on a specific epoxy resin of Buehler SamplKwick type, abraded with 1200-grit SiC paper using Metkon Digiprep ACCURA equipment, and finally mechanically polished using 6-μm, 3-μm, and 1-μm diamond paste and 0.03-μm colloidal silica on Buehler VibroMet2 equipment.

For all the obtained structural states of the studied alloys, conventional x-ray diffraction analysis was carried out at room temperature (RT, 298 K) using a PANalytical X'PertPRO MRD diffractometer with Cu K_{α} radiation (λ = 0.15418 nm) in the 2θ range from 30° to 90° in steps of 0.02° with an operating voltage and current of 40 kV and 30 mA, respectively. The rolling direction was set parallel to the direction of the x-rays projected onto the sample surface. The recorded XRD patterns were fit using PeakFit v4.11 software package to deconvolute the observed cumulative diffraction peaks and determine, for each constitutive peak, the position, intensity, and full-width at half-maximum (FWHM) broadening.

The evolution of the texture of the alloys during SPD was investigated by XRD analysis for the β-phase, using the same diffractometer equipped with a Euler cradle. The β-Ti (110), (200), and (211) pole figures (PFs) were plotted, then the raw PF data were fit and analyzed with a binning angle size of 5° × 5°, a Gaussian distribution, and ghost correction using the MTEX v3.2.2 software package.[23,24] The PFs were plotted considering the following crystallographic directions (sample reference frame): [100]—rolling direction (RD), [010]—transversal direction (TD), and [001]—normal direction (ND). Based on the PFs, inverse pole figures (IPFs) were calculated. For both alloys, only data referring to representative SPD states (for samples with the highest degree of deformation) are presented.

Microstructural SEM analysis was carried out using a TESCAN VEGA II—XMU. The analyzed samples were examined in three cross-sections/planes, RD–ND, TD–ND, and RD–TD. Due to the very large number of images obtained, only the most representative ones were selected for the proposed research objective. TEM/energy-dispersive spectroscopy (EDS) of the nanostructure obtained after SPD processing was carried out using a TECNAI G2 F30 S-Twin high-resolution (HR)TEM.

RESULTS AND DISCUSSION

Theoretical Analysis of β-Phase Stability of Studied Alloys Using the Bo–Md Diagram

The grain refinement of a β-Ti-based alloy during SPD depends on the possible types of structural deformation mechanism [dislocation slip or twinning of the β-phase or stress-induced martensitic (SIM) transformation], which, in turn, depends on the β-phase stability. Analysis of the β-phase stability of the alloys is thus important to anticipate the deformation behavior during the applied SPD process. The β-phase stability of the Ti-based alloys increases with increasing content of β-stabilizing elements, in this case Nb, Ta, and/or Zr. Practically, an equivalent concentration of Ti–Mo binary alloy—$[Mo]_{eq}$—is commonly used to determine the alloy stability.[25] Typically, an $[Mo]_{eq}$ value greater than 10 wt.% is regarded as sufficient to preserve the β-phase on quenching from above β-transus.[26]

For the two studied alloys, $[Mo]_{eq}$ is 12.5% for the TNT alloy and 10.1% for the TNTZ alloy. Being greater than and almost equal to 10 wt.%, these values indicate that both alloys should exhibit good β-phase stability. However, in recent years, attention has focused on analyzing the β-phase stability based on electronic parameters that describe the bonding characteristics of the β-phase, namely the bond order (Bo) and d-orbital energy (Md).[15,16] For a titanium alloy, the Bo and Md values are calculated using the compositional average of each parameter. As such calculations have recently been extended to include a variety of alloying elements, for the

present two alloys, the Bo and Md parameters were calculated using data from Ref. 16 for each alloying component (marked with as asterisk in Table I).

The Bo–Md diagram was developed from experimental data to predict the effects of alloy composition on the deformation behavior.[15,16] With decreasing β-phase stability, as reflected by an increase in Md or a decrease in Bo, the deformation mechanism changes, from left to right in the Bo–Md diagram, from (1) dislocation slip to (2) twinning and/or (3) martensitic transformation.[16] The parameter values (Bo and Md) calculated for the two studied alloys can thus be used to plot them on the Bo–Md diagram (Fig. 1) developed by Abdel-Hady et al.,[16] which represents an extension of the diagram of Morinaga[15] over a wider Bo range, specifically to include advanced β-stable alloys as promoted in recent years. Figure 1 shows the $\beta/(\beta + \alpha)$ and $(\beta + \alpha)/\alpha$ boundaries, together with the boundaries for Ms = RT (room temperature) and Mf = RT. Moreover, the dislocation slip (left area in Fig. 1), twin (middle area, between Ms and Mf), and martensite domains (right side of Mf curve), referring to the dominant deformation structural mechanisms that can occur during cold deformation of alloys, are indicated. Figure 1 generally shows that the position of an alloy moves as its composition changes.

In the Bo–Md diagram, the β-phase stability is higher when the Bo parameter is high and the Md parameter is low. The positions of the studied alloys on the Bo–Md diagram indicate high β-phase stability. The TNT alloy lies in the β domain (left side), very close to the $\beta/(\beta + \alpha)$ boundary, meaning that, besides high β-phase stability (as also indicated above by its $[\text{Mo}]_{eq}$ value of 12.5%), the dominant deformation mechanism is not determined conclusively due to its proximity to the border between dislocation slip, on the left, and twinning, on the middle. The position of the TNTZ alloy on the Bo–Md diagram, considering the vertical ascendant

extension of the Mf curve, corresponds to the border between the twinning and SIM deformation mechanisms, to the left and right, respectively. According to Refs.,[27–29] for an alloy with a solid-solution structure type, the twinning deformation mechanism may represent an important mode of initiation of grain refinement, similar to β-Ti alloys. These theoretical analyses reveal a general correlation between the β-phase stability and the deformation properties of β-Ti alloys, including the possible dominant deformation mechanisms, by demarcation of a frontier between the single β and biphase domains in the Bo–Md diagram.[16]

The Ms temperature for starting the martensitic transformation can be calculated using the formula from Ref. 30, which was determined with special reference to β-Ti alloys with high β stability. Thus,
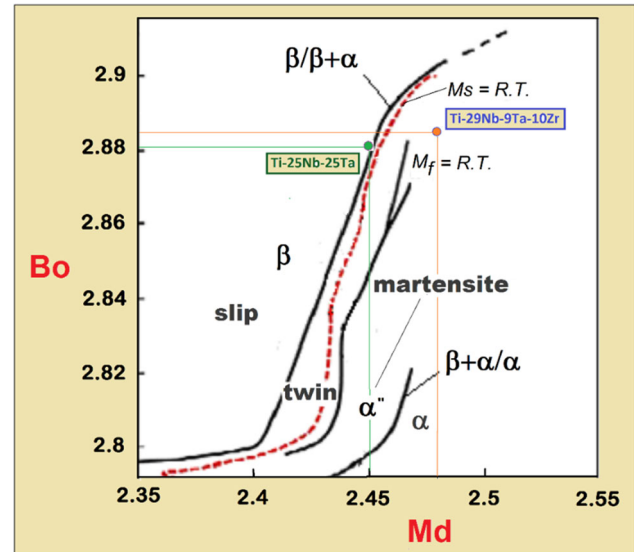

Fig. 1. Extended Bo–Md diagram with the positions of the two alloys marked (adapted from Ref. 16).

Table I. Chemical components and electronic parameters of each chemical component and the electronic parameters calculated for the studied alloys

Parameter	Ti	Nb	Ta	Zr
Bo	2.79*	3.099*	3.144*	3.086*
Md	2.447*	2.424*	2.531*	2.934*
TNT alloy				
wt.%	50	25	25	–
at.%	71.93	18,54	9.52	–
Calculated parameters for TNT alloy: B_o = 2.881 and M_d = 2.450				
TNTZ alloy				
wt.%	52	29	9	10
at.%	69.73	20.04	3.19	7.04
Calculated parameters for TNTZ alloy: B_o = 2.884 and M_d = 2.479				

*Data from Ref. 16

for the two studied alloys, the calculated Ms [K] values are

- For the TNT alloy: Ms [K] = 1156–17.6 Nb %gr. = 716 K = 443°C.
- For the TNTZ alloy: Ms [K] = 1156–17.6 Nb %gr.—41.2 Zr %gr. = 234 K = − 39°C.

These temperatures should be considered as estimates, because the formula from Ref. 30 contains various other possible alloying elements whereas, in the present case, only niobium and/or zirconium are included. These estimates can thus be considered as a starting point for future correlations with experimental data obtained from XRD analysis as well as SEM/TEM imaging.

Experimental Analysis of β-Phase Stability of Alloys

The structural characterization of the alloys was carried out using XRD analysis and SEM/TEM imaging. The resulting structural details are compared below with those discussed in the above-mentioned theoretical analysis, to evaluate the β-phase stability, the grain-refinement capability of each alloy during the SPD process, and additionally their plastic deformation behavior patterns.

Microstructural Analysis of Ti-29Nb-9Ta-10Zr Alloy

Phase Analysis Based on XRD Spectra Figure 2 presents the XRD profiles obtained after applying each processing step to the TNTZ alloy: firstly, the XRD spectra for the precursor sample, followed by those after each SPD/MPR step (MPR 20%, MPR

40%, MPR 60%, MPR 80%, and MPR 90%). Figure 2 shows that all the studied states had a majority β-Ti phase content with body-centered cubic structure in space group *Im3m*. The precursor sample contained only β-phase (Fig. 2a) as indicated by the observation of the intense (110)β and (211)β peaks as well as the (200)β peak, denoting high β-phase stability as provided by the large amount (48%) of β-stabilizing alloying elements.

The α''-Ti phase, with diffraction peaks marked (200), (130), (220), (202), and (021), represents the martensitic phase indexed in the C-centered orthorhombic system in space group *Cmcm*. However, all these diffraction peaks have much lower intensity in comparison with those of the β-phase, indicating that the α'' phase induced by SIM during the SPD/MPR process is not significant. In accordance with the position of this alloy in the Bo–Md diagram, i.e., at the border of twinning and SIM transformation, it seems that both mechanisms can be equally active. However, based on the experimental XRD data, it appears that the most active deformation mechanism is twinning, for two reasons: (1) the amount of orthorhombic α'' martensitic phase is very low (showing tiny peaks on the XRD spectra), denoting poor SIM transformation activity; (2) the β-grain dimension (Table II) decreased from 27.8 nm to 9.9 nm, denoting active β-grain refinement. Indeed, it is already known that the twinning process intensively aids grain refinement during the SPD process.[16,17,25–29]

Additionally, for the Ti-Nb-Ta-Zr system, the related literature shows that these various deformation structural mechanisms are the defining factors for achieving an alloy with a certain level
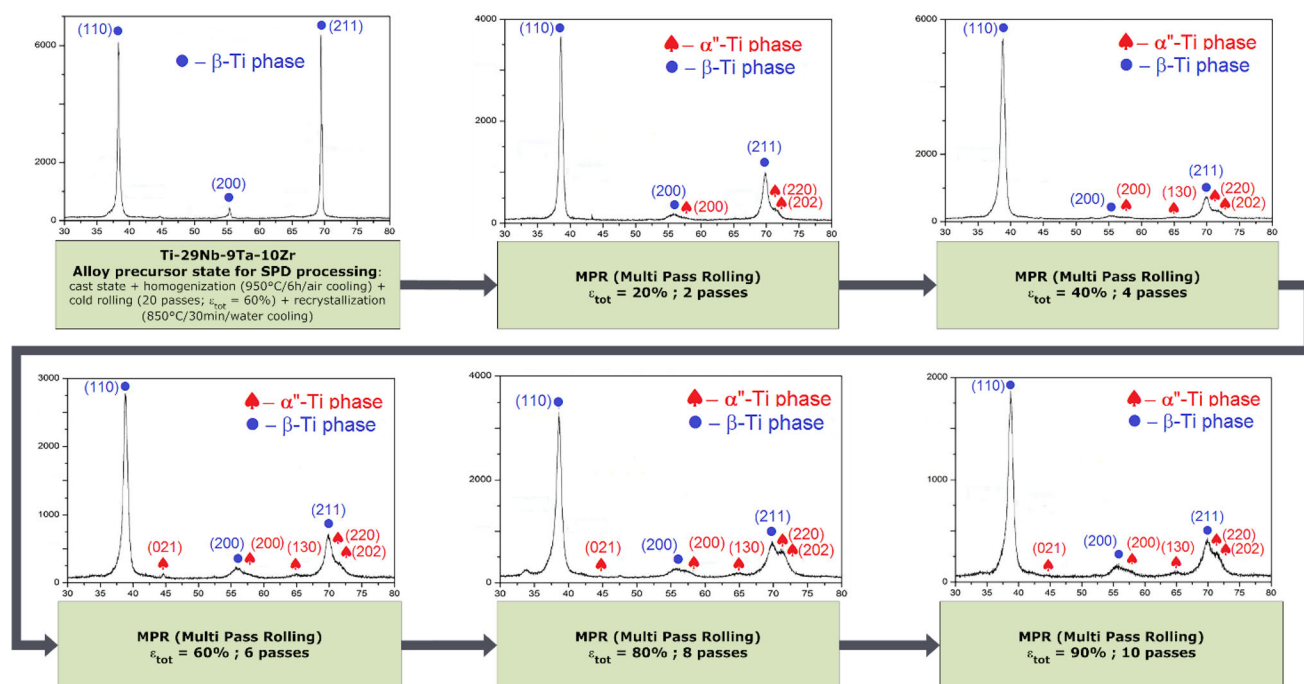

Fig. 2. XRD spectra of Ti-29Nb-9Ta-5Zr alloy processed by multipass rolling (MPR).

Table II. TNTZ alloy: crystallographic cell parameters of β-phase (*a*) and α″ phase (*a, b, c*), crystallite dimensions (*D*, nm), and microdeformation (ε, %) at crystalline network level

Structural State	β-Ti Phase			α″-Ti Phase		
	a [nm]	ε [%]	*D* [nm]	*a, b, c* [nm]	ε [%]	*D* [nm]
Initial state (Casting + homogenization + cold rolling + recrystallization)	0.330	0.05	27.80	*a* = 0.329 *b* = 0.478 *c* = 0.462	0.07	23.16
MPR (ε = 20%)	0.330	0.27	23.16	*a* = 0.323 *b* = 0.478 *c* = 0.460	0.22	13.90
MPR (ε = 40%)	0.330	0.25	10.69	*a* = 0.323 *b* = 0.479 *c* = 0.460	0.27	9.93
MPR (ε = 60%)	0.330	0.15	11.58	*a* = 0.321 *b* = 0.479 *c* = 0.459	0.37	34.75
MPR (ε = 80%)	0.330	0.17	9.93	*a* = 0.322 *b* = 0.479 *c* = 0.456	0.90	19.86
MPR (ε = 90%)	0.329	0.22	10.69	*a* = 0.321 *b* = 0.480 *c* = 0.456	0.92	23.16

of mechanical strength;[26–29] For example, for the alloys Ti-(13–26)Nb-(23–38)Ta and Ti-(13–35.5)Nb-(5–22)Ta-(4–7.2) Zr (in which the studied alloy can be framed), the volume fraction of α″ (which can increase the mechanical strength) is found to decrease with increasing Nb + Ta content.[29] In addition, the presence of Zr in the range from 4.1 wt.% to 4.6 wt.% is also observed to suppress α″ formation.[27–29] In the present case, the average dimension of the α″-phase, despite its low content, shows an interesting variation during the SPD process, from an initial value of 23.16 nm to a smaller one of 9.93 nm, and then again to a larger value of 34.75 nm. The explanation may be that the initially formed α″-grains (in the first step of the SPD procedure) decrease step-by-step during SPD, due to a crushing process; concomitantly, new α″-grains form in the subsequent stages of the SPD process, again with larger dimensions.

Based on these results, it can be considered that the most probable deformation mechanism of the TNTZ alloy during SPD is twinning, accompanied by grain refinement of the β saturated solid solution.[27–29] Meanwhile, SIM transformation can be considered to be a secondary, less active deformation mechanism, forming orthorhombic α″ martensite, although the evidence for this is very poor.[31–33]

Structural Parameters Obtained by XRD Analysis The XRD spectra recorded in each structural state were fit using the PeakFit v4.11 software package to determine the position, intensity, and FWHM peak-broadening parameters for each diffraction peak. The crystallographic cell parameters, crystallite dimensions for each identified phase, and microdeformation (ε, %) at the crystalline network level were also determined by using the FWHM parameter in the Williamson–Hall equation.[34] All these results are presented in Table II.

The cell parameter ($a\beta$) of β-phase remained essentially constant (0.330 nm), the deformation being accommodated mainly by twinning and less through martensitic transformation, which can occur with increasing degree of deformation. For the orthorhombic α″ phase, the three parameters $a\alpha''$, $b\alpha''$, and $c\alpha''$ showed very slight variation during the SPD process, probably occurring via some crystal lattice distortions.[35,36] Also, crystallographic texture may develop in highly deformed conditions, as briefly commented on in the next paragraph.

The essential result of the application of SPD is the advanced β-grain refinement, as shown by the approximately threefold decrease in the crystallite dimensions (Table II) from 27.8 nm to 9.9 nm. The influence of the α″ martensitic phase on the overall nanocrystalline appearance of the severely deformed alloy is probably minor because of its low content.

The results presented in Table II show that the microdeformation at the β-phase crystalline network level gradually decreased with increasing degree of deformation; thus, due to twinning accumulation followed by β-grain splitting and the gradual formation of a small amount of secondary α″, the internal stress and thereby the microdeformation decreased. In contrast, the

microdeformation corresponding to the α″ phase gradually increased with increasing degree of deformation, because of the tendency to accommodate α″ crystallites (even at their low content) among the β grains.

SEM Imaging of TNTZ Alloy The SEM images in Fig. 3a, b, c and d show the microstructure of the SPD/MPR-processed samples corresponding to the RD–ND cross-sections of the TNTZ alloy, verifying and validating the estimates obtained from the theoretical and XRD analyses above. From Fig. 3a, b, c and d, the degree of deformation applied by SPD/MPR gradually increases, from 20% to the final value of 90%. Note that the microstructure formed by the β-phase grains exhibits an increased twinning tendency (Fig. 3a and b) which favors the subsequent grain refinement. This observation provides experimental evidence for the supposed twinning of the β-phase as the main deformation

mechanism, coexisting to a lesser extent with SIM transformation.

Texture Analysis of TNTZ Alloy The texture analysis, for both alloys, was based on the calculation of the IPFs, which show the distribution of crystallographic directions parallel to the three sample directions, viz. [100]—rolling direction (RD), [010]—transversal direction (TD), and [001]—normal direction (ND) in the reference frame of the sample. Generally, IPFs are important for predicting the average properties of polycrystalline materials along selected directions.[22,37,38]

In the case of the TNTZ alloy, from among all the calculated IPFs, the sample with the highest degree of deformation (MPR 90%) was selected. Figure 4 shows the calculated IPFs corresponding to this sample status. From right to left, the distribution of crystallographic directions is represented, according to ND, TD, and RD, respectively. The IPFs in Fig. 4 reveal that the pairs [111]//ND and [110]//TD are representative, and the texture developed at this
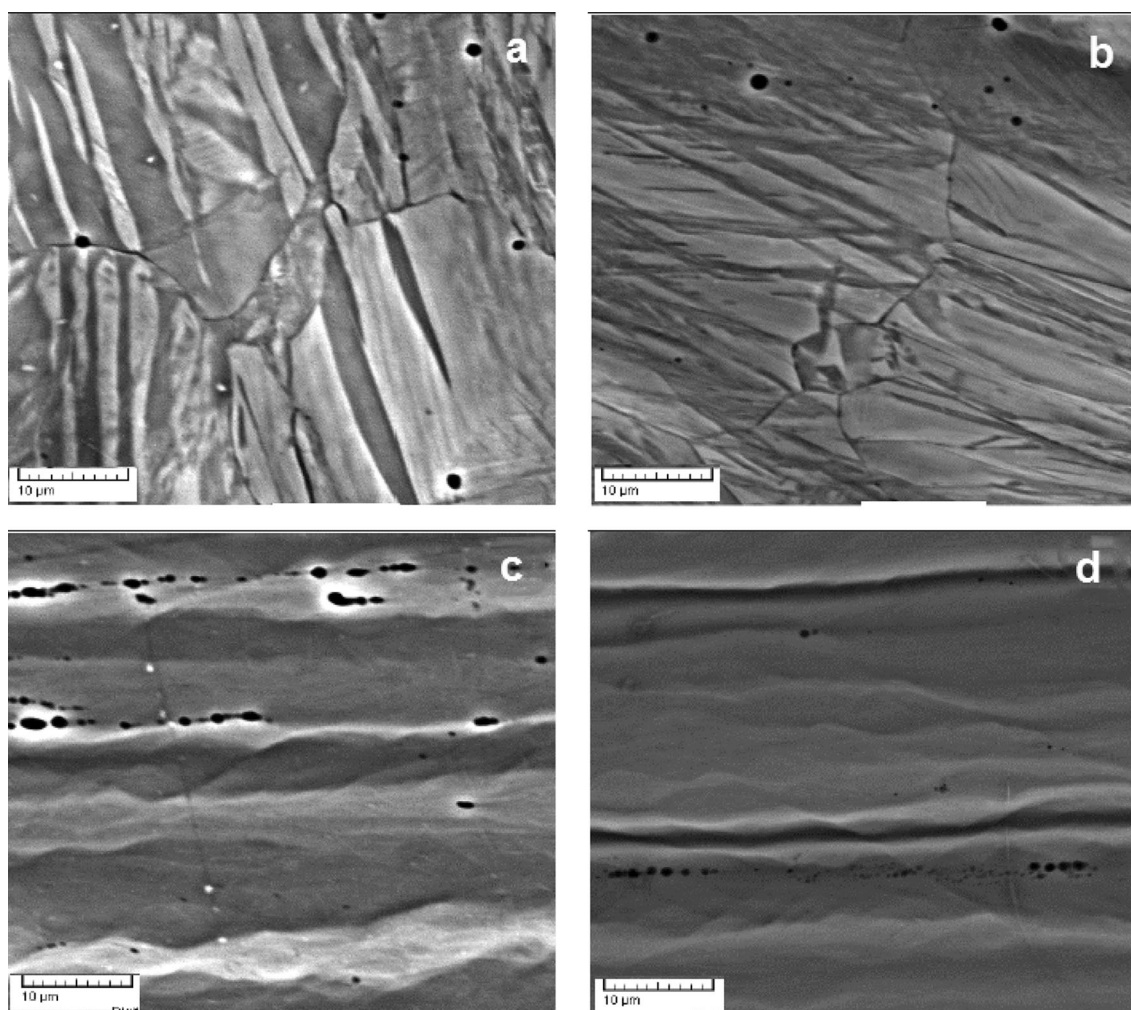

Fig. 3. SEM images of SPD-MPR processed TNTZ alloy (RD–ND cross-section): (a) MPR 20%, (b) MPR 40%, (c) MPR 80%, and (d) MPR 90%.
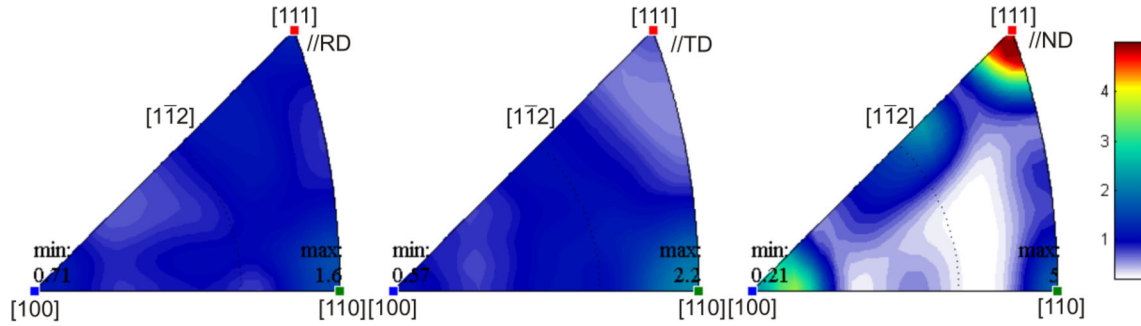
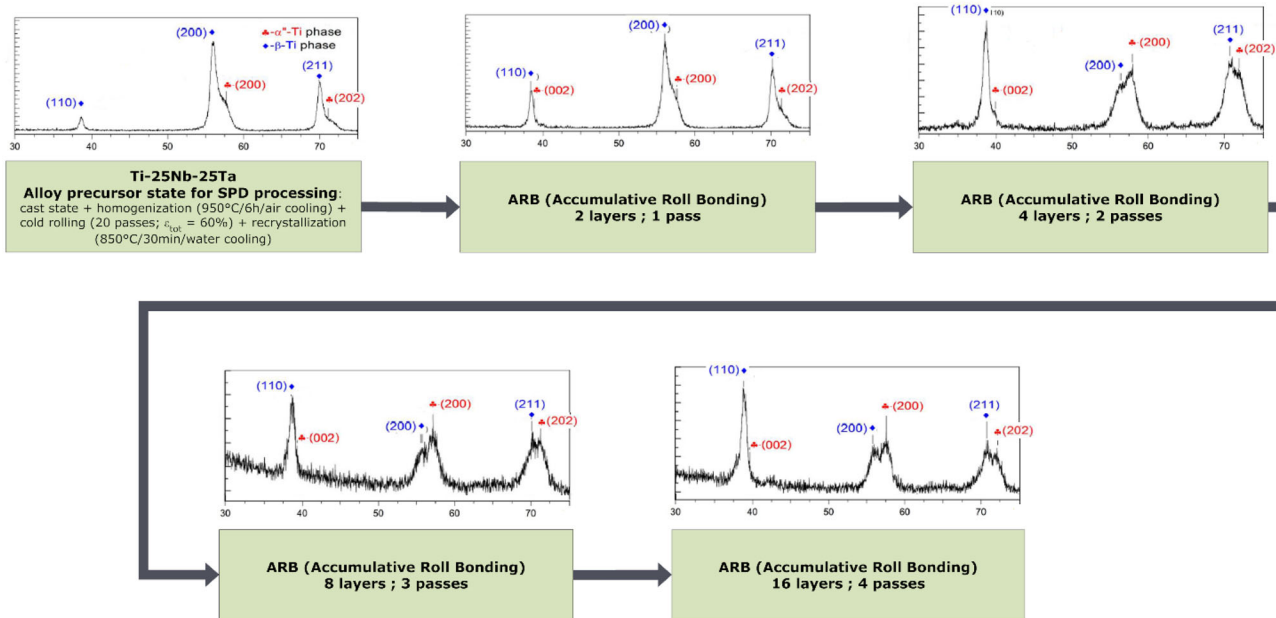Fig. 4. Representative inverse pole figures (IPFs) of TNTZ alloy (SPD/MPR 90%).

Fig. 5. XRD spectra for Ti-25Nb-25Ta alloy processed by ARB.

stage of the SPD/MPR process consisted of the formation of γ-fiber and ε-fiber, respectively.[38–40]

Microstructural Analysis of Ti-25Nb-25Ta Alloy

Phase Analysis Based on XRD Spectra Figure 5 presents the XRD profiles for the Ti-25Nb-25Ta alloy processed by SPD/ARB: firstly, the XRD spectra for the precursor sample, followed by the XRD spectra after the application of each ARB step. The β-phase is the majority, showing intense $(110)\beta$, $(200)\beta$, and $(211)\beta$ peaks, thus denoting high β-phase stability, as suggested by the high fraction (50%) of β-stabilizing alloying elements. The XRD spectrum of the precursor specimen reveals, besides the evident β-phase peaks, some other peaks corresponding to the α'' phase: $(002)\alpha''$, $(200)\alpha''$, and $(202)\alpha''$, which gradually become more evident as the ARB process progresses.

Furthermore, for the ARB specimens, the intensity of the β-phase diffraction peaks gradually decreased, finally becoming almost equal to those

corresponding to the α'' phase. Beginning with the ARB two-pass/four-layer step, the intensities of the $(200)\alpha''$ and $(202)\alpha''$ peaks become equal to those of the $(200)\beta$ and $(211)\beta$ peaks, indicating that an increased amount of α'' phase is induced during the SPD process. Another observation is related to the blurriness of the XRD profiles obtained after application of the final two ARB steps, which indicates severe grain deformation.

For β-Ti alloys in general, some literature reports that the dislocation slip and/or twinning are affected by changes in the electronic structures.[41–44] In addition, SIM transformation should also occur depending on the Ms level (which is relatively high at 443°C here). Therefore, some of these deformation mechanisms become dominant depending on the type and amount of alloying elements present. For the TNT alloy, considering the initial theoretical estimation based on the position of this alloy in the Bo–Md diagram at the border between dislocation slip and twinning, it seems that both of these

deformation mechanisms can be equally active. However, based on the XRD analysis, which reveals the formation of orthorhombic α″ martensitic phase during the SPD process, SIM transformation can be presumed to be an active deformation mechanism too. Instead, because the β-crystallite dimension remained practically unchanged during the SPD process, it can be presumed that the twinning mechanism did not act (or acted very little), because β-grain refinement did not occur. The initial β-grain was 29.4 nm, while by the end, it was 24.4 nm to 25.2 nm, indicating that a very small decrease occurred in comparison with the TNTZ alloy, for which the decrease was about three times greater. Consequently, dislocation slip and SIM transformation can be considered to be the main active deformation mechanisms.

Structural Parameters Obtained by XRD Analysis All the XRD profiles recorded for the TNT alloy were fit using the PeakFit v4.11 software package. The crystallographic cell parameters, crystallite dimensions for each identified phase, and microdeformation (ε, %) at the crystalline network level obtained by using the FWHM parameter in the Williamson–Hall equation[34] are presented in Table III.

For the TNT alloy, the cell parameter ($a\beta$) of the β-phase remained essentially constant. The average value of $a\beta$ for the TNT alloy (0.328 nm) was slightly smaller than that for the TNTZ alloy (0.330 nm) because of the absence of zirconium, which has a larger atomic radius compared with the other alloying elements. The three corresponding parameters $a\alpha″$, $b\alpha″$, and $c\alpha″$ of the martensitic α″

phase, with C-centered orthorhombic structure, also showed slight differences in comparison with those of the TNTZ alloy, resulting from the different chemical composition of the alloys.

In terms of β-grain refinement, the decrease of the crystallite dimensions (D, nm) is not so evident; the β-grain dimension decreased from 29.43 nm to 24.385 nm, i.e., by 14%, compared with 300% for the TNTZ alloy. A possible explanation for this result could be the greater content of α″-phase crystallites (about 40% after the last ARB step, and with nanometric dimensions of about 7 nm to 9 nm) as a consequence of SIM transformation, which facilitates more intense dislocation slip, favoring strong β-grain deformation without refinement.[12–14] In addition, the microdeformation corresponding to the α″ phase was generally higher than for the TNTZ alloy (1.589% compared with 0.458% on average) due to the greater amount of α″ phase. After the last ARB step, the microdeformation suddenly decreased, likely because of capping of the α″ formation, thus causing stress relaxation. Similarly, the microdeformation calculated at the level of the β-phase crystalline network was also higher than for the TNTZ alloy (1.055% compared with 0.185% on average) with low variations during SPD in general.

For the TNT alloy, the ability to form the martensitic α″-phase, as indicated above by the calculated Ms temperature of 443°C, is thus verified experimentally by the considerable amount of α″ phase formed. For the TNTZ alloy described above, with a much lower estimated Ms temperature of − 39°C, the lesser α″-phase formation was also

Table III. TNT alloy: crystallographic cell parameters of β-phase (a) and α″ phase (a, b, c), phase content (%), crystallite dimensions (D, nm), and microdeformation (ε, %) at crystalline network level

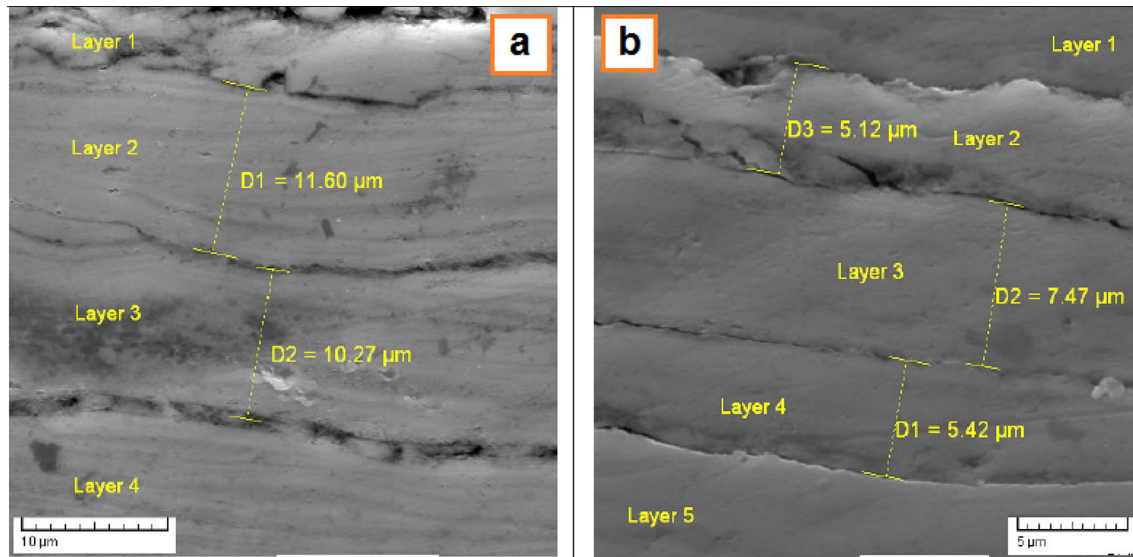| Structural State	Phase Content β-Ti/α″-Ti [%]	β-Ti Phase			α″-Ti Phase		
		a [nm]	ε [%]	D [nm]	a, b, c [nm]	ε [%]	D [nm]
Initial state Casting + homogenization + cold rolling + cecrystallization)	99.62 ± 0.23% 0.38 ± 0.11%	0.329	1.043	29.43	a = 0.319 b = 0.480 c = 0.463	2.043	8.766
ARB, two layers/one pass	–	0.328	0.984	28.532	a = 0.318 b = 0.481 c = 0.462	1.956	8.348
ARB, four layers/two passes	–	0.328	0.911	27.799	a = 0.318 b = 0.481 c = 0.462	1.775	8.176
ARB, eight layers/three passes	60.76 ± 1.09% 39.24 ± 0.64%	0.328	0.962	24.385	a = 0.318 b = 0.481 c = 0.462	2.100	7.315
ARB, 16 layers/four passes	58.94 ± 0.84% 41.06 ± 0.36%	0.328	1.375	25.271	a = 0.318 b = 0.481 c = 0.461	0.075	9.266

Fig. 6. SEM images of SPD/ARB-processed TNT alloy, corresponding to RD–ND cross-section: (a) ARB 8 layers; (b) ARB 16 layers.
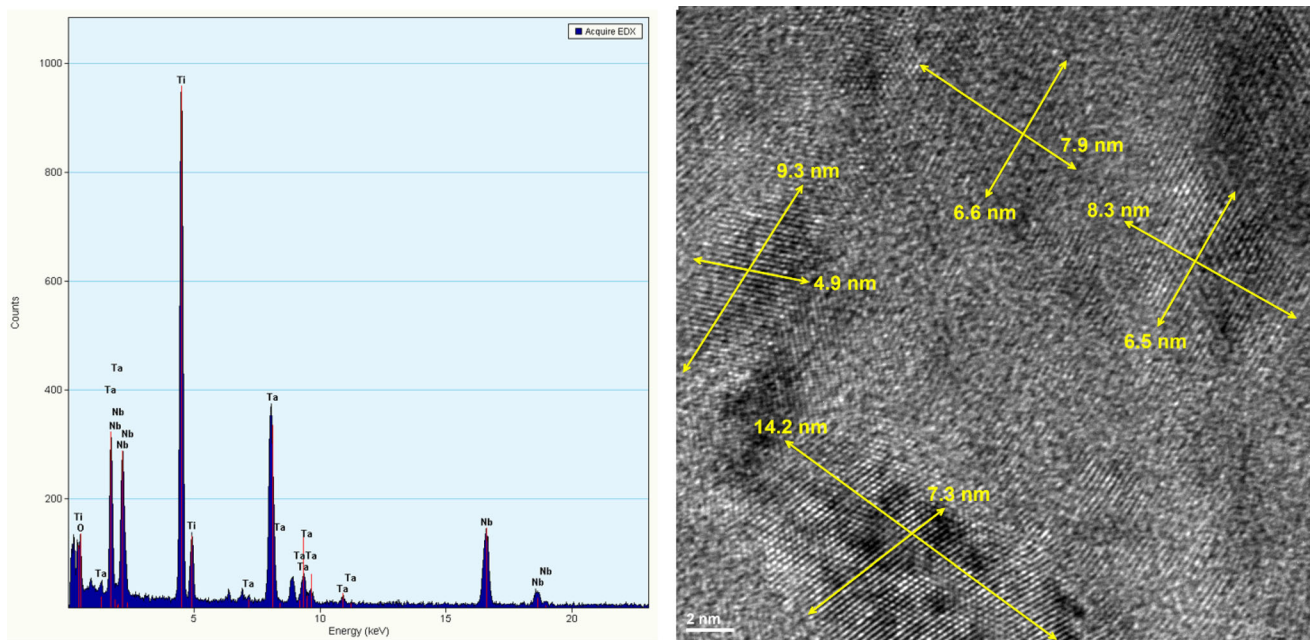

Fig. 7. TEM-EDS images of SPD/ARB-processed TNT alloy, corresponding to RD–ND cross-section: (a) EDS results; (b) ARB 16 layers.

verified experimentally by the XRD analysis, due to the very small amount of α'' phase detected.

SEM/TEM Microstructural Analysis of TNT Alloy The SEM microstructure of the SPD/ARB-processed samples corresponds to the RD–ND cross-section. The structures for the ARB three passes/8 layers and ARB four passes/16 layers are presented in Fig. 6a and b. Note that the formed layers are strongly elongated, without the presence of twinning phenomena. α''-Phase precipitates are not visible in the SEM images (Fig. 6a and b), due to

their nanoscale dimensions, but they are visible in the TEM image in Fig. 7b, which corresponds to the ARB 16-layer sample. The initial theoretical estimation for the TNT alloy regarding the presumed deformation mechanisms is in agreement with the XRD results, revealing a cumulative deformation mechanism (dislocation slip and SIM transformation), without twinning, as indicated by the lack of twinning phenomena in the SEM/TEM images.

Texture Analysis of TNT Alloy The evolution of the texture during SPD/ARB was investigated for the
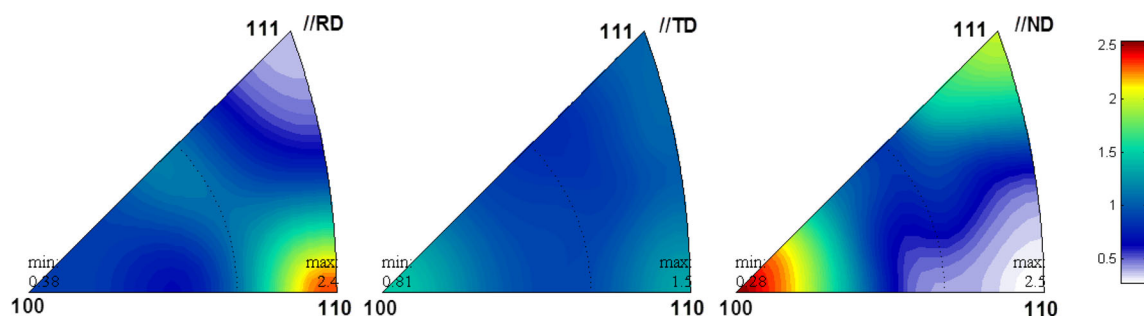
Fig. 8. Representation IPFs for TNT alloy (ARB 16 layers).

TNT alloy also. The IPFs corresponding to the state with the highest degree of deformation (ARB 16 layers) were selected for this presentation (Fig. 8). The IPFs in Fig. 8 show that the pairs [100]//ND and [110]//RD are representative, and the texture developed at this stage of the SPD/ARB process consisted of γ-fiber and α-fiber, respectively.[38–40]

In conclusion, it can be appreciated that, for the two studied alloys, the β-phase stability can be estimated theoretically using the [Mo]$_{eq}$ calculation, their position in the Bo–Md diagram, and the Ms calculation, although this only reveals the general features. Experimental validation of the estimated features and other detailed aspects concerning the β-phase stability was obtained by microstructural analysis based on XRD and SEM/TEM data acquisition and their detailed processing.

CONCLUSION

1. The evolution of the β-phase stability of two β-type Ti-based alloys during SPD processing was studied based on theoretical estimations and experimental results obtained by x-ray diffraction analysis and SEM/TEM imaging. The conditions for β-phase stability during SPD processing were established.
2. By using the [Mo]$_{eq}$ calculation, the position in the Bo–Md diagram, and the Ms temperature calculation, the β-phase stability was estimated theoretically; the specific deformation mechanisms active during the SPD process for each studied alloy and the ability for α″-phase formation through martensitic transformation were evaluated.
3. The crystallite dimensions, crystallographic cell parameters, and microdeformation at crystalline network level for each alloy at each stage of SPD were determined by XRD analysis. To verify the results, corresponding SEM/TEM images and texture analysis were added.
4. A development of the texture in the alloys during SPD processing accompanies the other analyzed transformations. The crystallographic texture strengthened during SPD, thus the orientation relationship was studied only for the states with the highest degree of deformation. The specific texture fibers for the β-phase were determined to be γ-fiber and ε-fiber for TNTZ alloy, and γ-fiber and α-fiber for TNT alloy.
5. Generally, comparison of the theoretical and experimental data revealed acceptable agreement in terms of: the good β-phase stability for both studied alloys; the deformation mechanism during the SPD process, mainly by twinning for the TNTZ-type alloy and a combination of dislocation slip with SIM transformation for the TNT-type alloy; and the variation of the crystallographic parameters.

ACKNOWLEDGEMENTS

REFERENCES

1. Y. Wang, J. Zhao, S. Dai, F. Chen, X. Yu, and Y. Zhang, *J. Mech. Behavior. Biomed. Mater.* 27, 33 (2013).
2. Y. Yang, S.Q. Wu, and G.P. Li, *Acta Mater.* 58, 2778 (2010).
3. J. Hwang, S. Kuramoto, T. Furuta, K. Nishino, and T. Saito, *J. Mater. Eng. Perform.* 14, 747 (2005).
4. L.Q. Wang, G.J. Yang, and H.B. Yang, *Rare Metal Mater. Eng.* 38, 0579 (2009).
5. Y. Zheng, R.E.A. Williams, S. Nag, R. Banerjee, H.L. Fraser, and D. Banerjee, *Scr. Mater.* 116, 49 (2016).
6. H. Wang, X. Yuan, K. Wu, C. Xu, Y. Jiao, W. Ge, and J. Luo, *J. Mater. Process. Tech.* 255, 76 (2018).
7. D. Raducanu, V.D. Cojocaru, A. Nocivin, I. Cinca, N. Serban, and E.M. Cojocaru, *JOM* 71, 264 (2019).
8. M. Niinomi, M. Nakai, M. Hendrickson, P. Nandwana, T. Alam, D. Choudhuri, and R. Banerjee, *Scr. Mater.* 123, 144 (2016).
9. J.I. Qazi, B. Marquardt, and H.J. Rack, *JOM* 57, 5 (2005).
10. D. Raabe, B. Sander, M. Friák, D. Ma, and J. Neugebauer, *Acta Mater.* 55, 4475 (2007).
11. D. Zhao, T. Ebel, M. Yan, and M. Qian, *JOM* 67, 2236 (2015).
12. I. Kopova, J. Stráský, P. Harcuba, M. Landa, M. Janeček, and L. Bačákova, *Mater. Sci. Eng., C* 60, 230 (2016).
13. L.A. Matlakhova, A.N. Matlakhova, S.N. Monteiro, S.G. Fedotov, and B.A. Goncharenko, *Mater. Sci. Eng., A* 393, 320 (2005).
14. Y.L. Zhou, M. Niinomi, and T. Akahori, *Mater. Sci. Eng., A* 371, 283 (2004).

15. M. Morinaga, N. Yukawa, T. Maya, K. Sone, and H. Adachi, Theoretical design of titanium alloys, in *Sixth World Conference on Titanium: Proceedings*, Cannes, June 6–9, 1988, Société Française de Metallurgié, edited by P. Lacombe, R. Tricot, and G. Beranger, Cedex, France: Les Editions de Physique, ©1989.
16. M. Abdel-Hady, K. Hinoshita, and M. Morinaga, *Scr. Mater.* 55, 477 (2006).
17. R.P. Kolli, W.J. Joost, and S. Ankem, *JOM* 67, 1273 (2015).
18. H.Y. Kim, S. Hashimoto, J.I. Kim, T. Inamura, H. Hosoda, and S. Miyazaki, *Mater. Sci. Eng., A* 417, 120 (2006).
19. J. Sun, Q. Ke, and W. Chen, *J. Mater. Process. Technol.* 264, 119 (2019). https://doi.org/10.1016/j.jmatprotec.2018.09.002.
20. I.P. Semenova, A.V. Polyakov, V.V. Polyakova, Y. Huang, R.Z. Valiev, and T.G. Langdon, *Adv. Eng. Mater.* 18, 2057 (2016).
21. M.J. Kriegel, M. Rudolph, A. Kilmametov, B.B. Straumal, J. Ivanisenko, O. Fabrichnaya, H. Hahn, and D. Rafaja, *Metals* 10, 402 (2020). https://doi.org/10.3390/met10030402.
22. D. Raducanu, V.D. Cojocaru, A. Nocivin, D.M. Gordin, and I. Cinca, *Mater. Sci. Eng., A* 689, 25 (2017).
23. F. Bachmann, R. Hielscher, and H. Schaeben, *Solid State Phenom.* 160, 63 (2010).
24. F. Bachmann, R. Hielscher, P.E. Jupp, W. Pantleon, H. Schaeben, and E. Wegert, *J. Appl. Crystall.* 43, 1338 (2010).
25. T. Zhou, M. Aindow, S.P. Alpay, M.J. Blackburn, and M.H. Wu, *Scr. Mater.* 50, 343 (2004).
26. P.J. Bania, *J. Metal* 41, 16 (1994).
27. J. Azadmanjiri, C.C. Berndt, A. Kapoor, and C. Wen, *Crit. Rev. Solid State Mater. Sci.* 40, 164 (2015). https://doi.org/10.1080/10408436.2014.978446.
28. X.Y. Shi, Y. Liu, D.J. Li, B. Chen, X.Q. Zeng, J. Lu, and W.J. Ding, *Mater. Sci. Eng., A* 630, 146 (2015).
29. C.X. Ren, Q. Wang, Z.J. Zhang, Y.K. Zhu, and Z.F. Zhang, *Acta. Metall. Sin. (Engl. Lett.)* 30, 212 (2017).
30. S. Neelakantan, R. Rivera-Diaz-del-Castillo, and S. van der Zwaag, *Scr. Mater.* 60, 611 (2009).
31. N. Sakaguchi, M. Niinomi, T. Akahori, J. Takeda, and H. Toda, *Mater. Sci. Eng., C* 25, 363 (2005).
32. N. Sakaguchi, M. Niinomi, T. Akahori, J. Takeda, and H. Toda, *Mater. Sci. Eng., C* 25, 370 (2005).
33. M. Geetha, A.K. Singh, R. Asokamani, and A.K. Gogia, *Prog. Mater Sci.* 54, 397 (2009).
34. L.R. Ribeiro, R.C. Junior, F.F. Cardoso, R.B.F. Filho, and L.G. Vaz, *J. Mater. Sci.* 20, 1629 (2009).
35. N.V. Kazantseva, V.P. Pilyugin, S.E. Danilov, and VYu Kolosov, *Phys. Metals Metallogr.* 116, 501 (2015).
36. Y. Horiuchi, T. Inamura, H. Young Kim, S. Miyazaki, K. Wakashima, and H. Hosoda, *Mater. Trans.* 47, 1209 (2006).
37. A. Nocivin, D. Raducanu, I. Cinca, C. Trisca-Rusu, M. Butu, I. Thibon, and V.D. Cojocaru, *J. Mater. Eng. Perform.* 24, 1587 (2015).
38. M. Holscher, D. Raabe, and K. Lucke, *Acta Metall. Mater.* 42, 879 (1994).
39. D. Raabe and K. Lucke, *Mater. Sci. Technol.* 9, 302 (1993).
40. B. Sander and D. Raabe, *Mater. Sci. Eng., A* 479, 236 (2008).
41. D. Kuroda, M. Niinomi, M. Morinaga, Y. Kato, and T. Yashiro, *Mater. Sci. Eng., A* 243, 244 (1998).
42. M. Abdel-Hady Gepreel and M. Niinomi, *J. Mech. Behav. Biomed. Mater.* 20, 407 (2013).
43. S. Ozan, J. Lin, Y. Li, and C. Wen, *J. Mech. Behav. Biomed. Mater.* 75, 119 (2017).
44. M. Gouda, M. Abdel-Hady Geprel, K. Yamanaka, H. Bian, K. Nakamura, and A. Chiba, *JOM* (2019). https://doi.org/10.1007/s11837-019-03690-7.